# Experimental Validation of Time Reversal Multiple Access for UWB Wireless Communications at the SubTHz Frequency Band

Ali Mokh, Julien de Rosny, George Alexandropoulos, Mohamed Kamoun, Abdelwaheb Ourir, Ramin Khayatzadeh, Arnaud Tourin, Mathias Fink

# Experimental Validation of Time Reversal Multiple Access for UWB Wireless Communications at the SubTHz Frequency Band

Ali Mokh[1], Julien de Rosny[1], George C. Alexandropoulos[2],
Mohamed Kamoun[3], Abdelwaheb Ourir[1], Ramin Khayatzadeh[3], Arnaud Tourin[1], and Mathias Fink[1]

[1]ESPCI Paris, PSL Research University, CNRS, Institut Langevin, France
[2]Department of Informatics and Telecommunications, National and Kapodistrian University of Athens, Greece
[3]Mathematical and Algorithmic Science Lab, Paris Research Center, Huawei Technologies France
emails: firstname.lastname@espci.fr, alexandg@di.uoa.gr, firstname.lastname@huawei.com

***Abstract*—Increase data rate while having low power consumption and low computational complexity at the receiver are the key elements for the research in wireless communication for low complexity devices. Sub Terahertz (SubTHz) radio-frequency domain can support ultra-wideband (UWB) communications, and thus the unprecedented increase in the wireless network capacity, that could be the next breakthrough for the next 6G standards. However, the technology of subTHz transceivers is not yet completely mature to apply the same advanced processes as the ones that are currently implemented for microwaves communications. We propose to test the effectiveness of Time Reversal (TR) precoding which is simple and robust processing to focus on time and space UWB waveforms in exploiting the channel diversity. In this paper, we first investigate experimentally the performance of subTHz TR focusing on multiple access transmission scenarios at a high data rate, while keeping the receiver simple and with low computational complexity.**

***Index Terms*—Time Reversal, low-complexity reception, pulse position modulation, THz communications, UWB.**

## I. Introduction

Internet of Things (IoT) technologies offer advanced services in different domains such as medicine, power, connected-smart cities, smart homes, agriculture, etc. Some of the main requirements of the IoT are the support of massive deployment, scalability, high efficiency, low power consumption, and intermittent connectivity. An important part of the IoT network is the wireless network which needs to support low-power devices equipped with very low complexity transceivers [1], [2], [3]. Various communication strategies have been proposed to limit the energy consumption of the communication modem of IoT devices both from software and hardware perspectives [3], [4]. In particular UWB waveforms have ushered in a new era in short-range wireless communications for wireless sensor networks, by enabling both robust communications and accurate ranging capabilities [5]. To support large bandwidth for multiple devices, the initial discussion indicates that frequencies in the range of subTHz and above will be considered for 6G as there are plenty of available bands suitable to satisfy these requirements [6], [7]. It appears that 6G will utilize a spectrum beyond 140GHz with particular applications in very short-range communication or 'whisper radio' [8]. One central issue facing UWB waveforms for low complexity devices is to effectively collect energy that is dispersed in rich multi-path channels. TR appears to be a paradigm shift in exploiting this rich multi-path to focus in time and space UWB pulses [9] while shifting the complexity to the transmitter side. In [10], TR was considered in UWB communications. The increasing of SNR thanks to temporal focusing have been experimentally verified with a multi-antenna transmitter [11], [12], [13]. The concept of TR division multiple access was introduced in [14] for multiuser communication. Very recently, we evaluated the performance of TR in the subTHz domain in[15] for spatio-temporal focusing, and we used the experimentally measured signals in a simulation chain to simulate data transmission using spatial modulation.

In this paper, we propose to experimentally evaluate the capability of TR in the sub-THz domain for multiple access transmission, for low complexity devices, and at a high data rate. An experimental setup is used to perform the channel estimation and time-reversal transmission at 273.6 GHz carrier frequency and with a bandwidth up to 2 GHz, where the link between the transmitter and the receiver is a waveguide with a tilted incident angle. We selected two different positions for the receiver as 2 different receivers, and we transmitted binary data using a modulation technique that depends on the position of the peak of the received signal. The detection was performed via two incoherent receivers with a simple power detector.

The rest of the paper is organized as follows. In section II, the principle of TRDMA is described. In section III, we present the subTHz experimental setup to estimate the channels and to measure the TR signals in multiple access. In section IV, we present the experimental results for data transmission for different data rates. Finally, section V is devoted to the conclusion.

## II. Time Reversal Division Multiple Access

We consider a multi-access wireless communication system comprising one transmitter that is equipped with a single

antenna element and communicates in the downlink direction toward $N$ single-antenna. We represent by $h_i[k]$ the baseband channel impulse response (CIR) at discrete time $k$ between the transmitter and the $i$-th ($i = 1, 2, \ldots, N$) receiving antennas. TR preprocessing consists of using the time reversed CIR, i.e., $h_i^*[L-k]$ to focus the electromagnetic field on the $i$-th antenna. As a consequence, the signal sent by the transmit antenna to focus individually the baseband message $x_i[l]$ on each receiving antenna is given by

$$s[k] = \sum_{i}^{N} \frac{\sum_l x_i[l] h_i^*[L+l-k]}{\sqrt{\sum_l |h_i[l]|^2}}, \tag{1}$$

where it is assumed that the CIR is composed of $L$ significant taps. The normalisation ensures that the power emitted toward each user is the same.

Typically, the symbol rate can be lower than the system CIR rate. Considering $T_p$ be the pulse duration used to estimate the channel and to perform the TR precoding. $T_p$ is related to the system bandwidth $B$, where $T_p = 1/B$. And let $D$ be the rate backoff factor that is introduced to match the symbol rate with the pulse duration, then the symbol duration is $T_s = DT_p$. Then, the signal received by each antenna is sampled every $T_s = DT_p$ seconds at $t = kDT_p$, in order to detect the symbol $x[k]$:

$$y_j[k] = y[t = kDT_p] = \sum_{l}^{L} \sum_{i}^{N} x_i[l] R_{j,i}[L + l - kD] + n_j[k]. \tag{2}$$

where the expression of the correlation function between the CIRs of users $j$ and $i$ is given by

$$R_{j,i}[k] = \frac{\sum_{m,k'} h_{i,m}^*[k-k'] h_{j,m}[k']}{\sqrt{\sum_{m',l} |h_{i,m'}[l]|^2}}, \tag{3}$$

and $n_j[\cdot]$ is the zero-mean additive white Gaussian noise with standard deviation $\sigma$ at user $j$.

TR precoding aims to focus the received signal in time and space at the targeted receive antenna by applying its time reversed CIR [16], and we can see from equation 3 that the auto-correlation function has a real-value peak at $R_{i,i}[0]$. This is referred to the fact that all the $M \times L$ signals add up coherently at this time and location ($R_{i,i}[0] = \sqrt{\sum_{m',l} |h_{i,m'}[l]|^2}$).

However, the imperfect space-time focusing of the TR precoding produce 2 kinds of interference:

- ISI from the signals that add incoherently at the same antenna $i = j$ in the time that is different than 0, i.e. $R_{i,i}[k]$ for $k <> 0$.
- IUI from all the signals in the auto-correlation function for $i \neq j$.

## III. SubTHz Experimental Measurements

In this section, the TR focusing and TRDMA transmission in the sub-THz domain are tested experimentally. In such frequencies, the attenuation of the channel becomes very high, and it is difficult to have a multi-path channel even for indoor application. So we prepared a specific setup for the experiment to be able to create a multi-path channel.

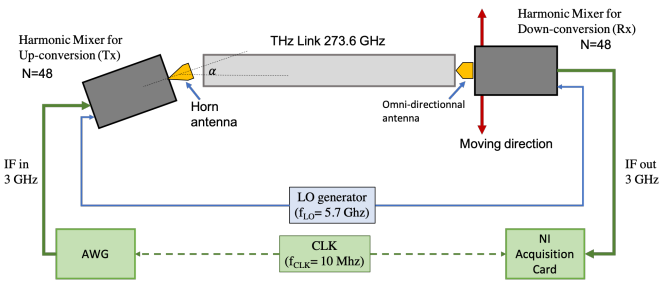


Figure 1. SubTHz Experiment Setup

### A. Experiment Setup

Our experimental setup at $f_c = 273.6$ GHz using an aluminum tube as a waveguide to create a multi-path channel is shown in Fig. 1. The diameter of the cylindrical waveguide considered here equals 7mm, i.e., about 10 times the wavelength, and its length is 1 m. The heart of the experimental set-up is 2 Spectrum/Signal Analyzer Extension Modules (SAXs) by Virginia Diodes, Inc. One of them is used to upconvert an intermediate frequency (IF) signal of 3 GHz generated by an I/Q modulation generator to a carrier frequency of 273.6 GHz. This last is obtained thanks to the multiplication by a factor $N$ =48 of the frequency of a local oscillator working at 5.7 GHz. On the receiving side, the same local oscillator still multiplied by a factor of 48 allows to down-convert to an IF signal, the field received by an omnidirectional antenna. This signal is sampled by a waveform digitizer. The modulation generator and the waveform digitizer are synchronized by a 10 MHz reference clock. The bandwidth is limited to 2 GHz by the modulation generator. Instead of directly dealing with IF signals, for convenience, the recorded signals are numerically down-converted into in-phase and quadrature-phase pairs of signals. Each time step that lasts the inverse of the I/Q modulator bandwidth is called tap. For the transmitter, we use a diagonal horn antenna provided by Virginia Diodes, Inc. To probe the focal spot at the waveguide extremity, the dipole antenna is mounted on a linear stepper motor stage.

### B. Channel Estimation and Time Reversal Focusing

The estimation of the CIR and TR precoding was performed as follows. First, a chirp signal spanning the range [$f_c - B/2$ $f_c + B/2$] is transmitted by the Tx. Synchronously, the signal is probed by the Rx antenna. The computer performs the CIR estimation by correlating the recorded signal with the chirp signal. Even if TR generates high amplitude pulses, the gain is not sufficient to directly probe the pulse with an Rx antenna. For this reason before emission, the CIR flipped in time is also convoluted with the same chirp signal. Similar to the CIR estimation, the TR-focused signal is reconstructed in the computer by cross-correlation. The results of the channel estimation and the TR received signals for 2 GHz bandwidth are shown in Figure 2.

Thanks to the waveguide, the rays coming from the transmitter that is inclined of angle $\alpha$ from the direction of the

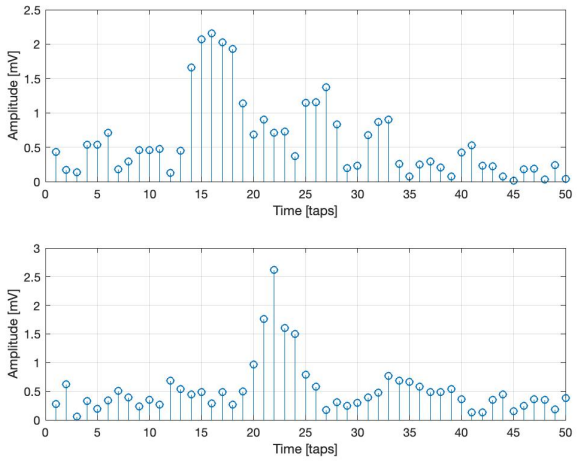


Figure 2. Channel Impulse response and Time reversed signal at B=2GHz

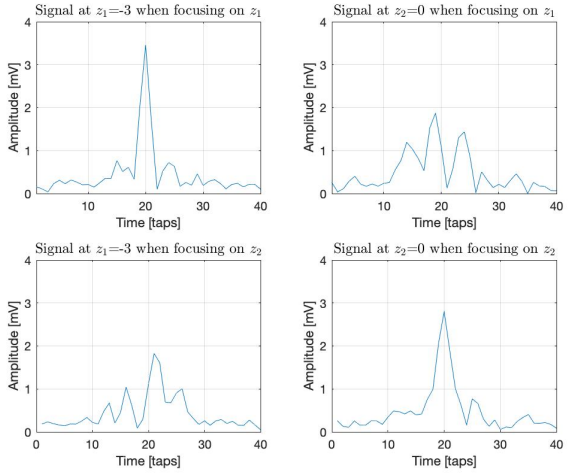


Figure 3. Baseband received signals at the two spatial positions $z_1 = -3mm$ and $z_2 = 0$ when applying TR to focus towards $z_1$ or $z_2$.

tube, will have different path distances because of their reflections inside the tube. This phenomenon creates the multipath channel that is probed at the receiver side and shown in the top sub-figure of Figure 2. The bottom sub-figure shows the received TR signal that is focused in time with a higher central peak.

### C. Multiple Access Measurements

We measured the CIR for different positions of the Rx antenna spaced by 1 mm between $x$ =-3mm to 3 mm, where $x = 0$ is the position facing the center of the tube output, using a bandwidth $B$= 2 GHz. We then select two positions where the CIRs are less correlated, namely $z_1 = -3$ mm and $z_2 = 0$, to apply the TR precoding for multiple access transmission. Fig. 3 shows the baseband received signals at the two spatial positions $z_1$ and $z$ when applying TR to focus towards $z_1$ or $z_2$, i.e. the focusing signal and the IUI when targetting one of the two positions. A peak signal localized in time appears at the targeted position (for the two positions). The figure shows the capability of the TR to focus the signal in time and space at the targeted position.

To investigate the capability of transmitting data in multiple access scenarios, we use the same scenario to modulate binary data with the focusing signal using a modulation technique that is explained in the next section.

## IV. Pulse Position Modulation in TRDMA

In this section, we perform experimental measurements that apply the TR precoding for data transmission. The binary data is transmitted using the Pulse Position Modulation (PPM).

### A. System Model

The idea is to use the TR precoding to target two spatial positions, to transmit two data streams at the same time and frequency, by exploiting the channel spatial diversity. As explained in the previous section, we convoluted the reversed signal (for TR precoding) by a chirp to increase its energy, since we are limited by the maximum power of the transmitter, and so the duration of each symbol is related to the chirp duration. For this purpose, we propose to use PPM modulation to code the binary information, where the position of the maximum amplitude of the received signal (or the maximum of $R_{i,j}[k]$ in equation 3) will code the information.

Let $\tau_c$ be the chirp length in taps (i.e. the time duration of the chirp is $\tau_c/B$ seconds), $D$ be the rate backoff, and $n$ is the order of the PPM modulation or the number of bits per chirp. So the modulation with TR multiple access to transmit data two positions $z_1$ and $z_2$ is performed as follow:

- The baseband CIR of each corresponding $z_i$ are flipped in time and convoluted with a chirp each.
- The corresponding $n_i$ bits to be transmitted for each receiver is converted to an integer $m_i$ that represents the corresponding position, and then the previously precoded signals are rotated by circular rotation with $m_i$ taps and transmitted after normalization.
- At the receiver side, the receiver has to estimate the position of the peak to decode the information. A simple power detector for each receiver can detect the position.

The motivation is to show the capability of TR in the sub-THz domain to spatial multiplexing, with a very simple receiver that does not need phase detection and synchronization between antennas.

In our experiment, we evaluated the transmission for different data rates that correspond to a different order of modulation and chirp length. The data rate to 2 users can be calculated as follow:

$$\text{Bit Rate} = 2 \times \frac{Bn}{\tau_c}. \tag{4}$$

Table I shows the different configurations of chirp length and the order of modulations that have been used in the experiment, as well as their corresponding bit rate. Figure 4 shows the received signals at two positions $z_1 = -3$ mm and $z_2 = 0$ mm, when using a chirp of $\tau_c = 40000$ at 2 GHz bandwidth (i.e. the duration of the chirp is 20 $\mu s$). The order of modulation is $n = 10$ and $D = 39$ for each receiver. We

Table I
CORRESPONDING DATA RATE FOR MODULATION CONFIGURATION

| Chirp length [taps] | bit per chirp | Bit Rate [Mbps] |
|---|---|---|
| 70 | 6 | 343 |
| 300 | 8 | 107 |
| 1100 | 10 | 36.4 |
| 2200 | 10 | 18 |
| 4000 | 10 | 10 |
| 40000 | 10 | 1 |

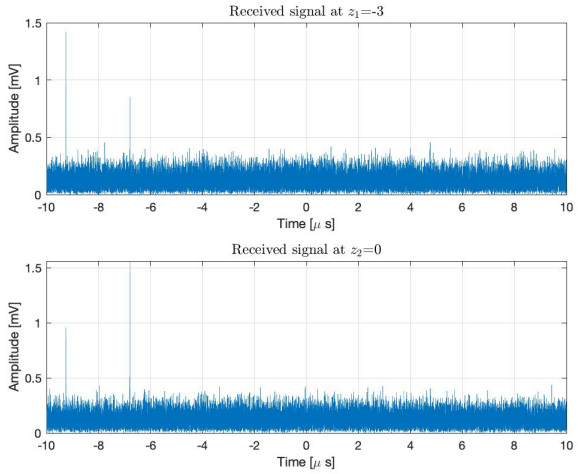


Figure 4. Received signals at positions $z_1 = -3mm$ and $z_2 = 0$ when applying TRDMA with PPM.

can see that for each spatial position, the received signal has a maximum value at the temporal position that corresponds to the transmitted PPM symbol, and the second peak is the interference from the signal of the other position (inter-user interference).

### B. Simulation Results

We used the signals from the measurement section, and we calculate the signal and the interference at the two positions $z_1 = -2.7$ mm and $z_2 = -1.8$ mm, and for different $D$.

Fig. 5 shows the SINR of the received signal at each position in terms of the bit rate that is calculated in Table I. It is shown that the SINR of the signal degrades with a higher bit rate, and this is referred to the combination of two factors: the first one is the length of the chirp that decreases with a higher bit rate, and so the energy transmitted per symbol is reduced. The second factor is the rate backoff that is reduced in case of saturation of the order of modulation for a certain chirp length (if the chirp is 1100 taps and the order of modulation is 10 bits per symbol, then we have one position per tap). In addition, even for a high data rate, the SINR remains greater than 0 dB, and this shows the capability for the multiple access transmission of the TR in the subTHz domain. These experiments are done in offline (non-real time measurements), and the CIR estimation is maintained through the computer that connects the transmitter and the receiver. The goal is to show the capability of transmission in high data rate while

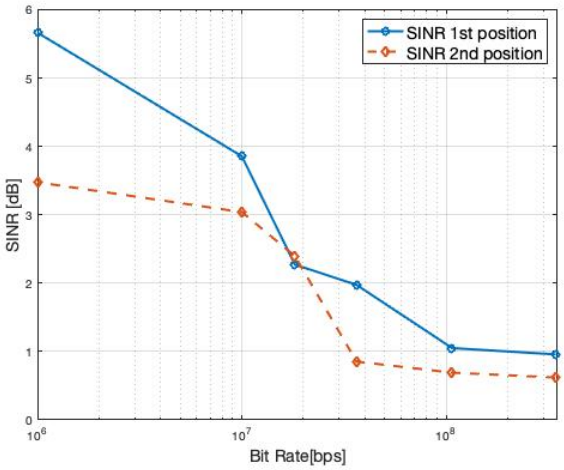


Figure 5. SINR at the 1st and 2nd position for different data rate.

keeping the receiver simple. In future work, a real channel estimation with disconnected transmitter and receiver should be considered. For this reason, and to keep the receiver simple, the channel estimation protocol should take into account that the receiver is incoherent (no complex data is generated).

## V. CONCLUSION

In this paper, we investigated the capability of TR-based precoding for multiple access transmission in the subTHz frequency band. An experimental setup with a waveguide at the carrier frequency 273.6 GHz with 2 GHz transmission bandwidth has been designed and realized to first estimate the channel, and then for performing TRDMA. In particular, the channel estimation at two different positions separated by 3 mm has been used for multiple access transmission. The presented results validated the capability of TR for multi-user communications in subTHz frequencies, and showcased data communication with simple PPM detection exceeding 340 Mbps. In the future, we intend to consider reconfigurable intelligent surfaces [17] for reprogrammable rich scattering conditions, enabling TR-based THz wireless communications.

## REFERENCES

[1] K. Georgiou, S. Xavier-de Souza, and K. Eder, "The IoT energy challenge: A software perspective," *IEEE Embedded Syst. Lett.*, vol. 10, no. 3, pp. 53–56, Sep. 2018.
[2] G. Luo, B. Guo, Y. Shen, H. Liao, and L. Ren, "Analysis and optimization of embedded software energy consumption on the source code and algorithm level," in *Proc. IEEE Int. Conf. Embedded Multimedia Comput.*, Jeju, South Korea, Dec. 2009, pp. 1–5.
[3] C. Gray, R. Ayre, K. Hinton, and R. S. Tucker, "Power consumption of IoT access network technologies," in *Proc. IEEE ICC*, London, UK, Jun. 2015, pp. 2818–2823.
[4] J. Henkel, S. Pagani, H. Amrouch, L. Bauer, and F. Samie, "Ultra-low power and dependability for IoT devices," in *Proc. IEEE Design, Autom. & Test Europe Conf.*, Lausanne, Switzerland, Mar. 2017, pp. 954–959.
[5] J. Zhang, P. V. Orlik, Z. Sahinoglu, A. F. Molisch, and P. Kinney, "UWB systems for wireless sensor networks," *Proc. IEEE*, vol. 97, no. 2, pp. 313–331, Feb. 2009.
[6] W. Saad, M. Bennis, and M. Chen, "A vision of 6G wireless systems: Applications, trends, technologies, and open research problems," *IEEE Network*, pp. 1–9, Oct. 2019.

[7] F. Tariq, M. R. Khandaker, K.-K. Wong, M. A. Imran, M. Bennis, and M. Debbah, "A speculative study on 6G," *IEEE Wireless Commun.*, vol. 27, no. 4, pp. 118–125, Aug. 2020.

[8] Y. Xing and T. S. Rappaport, "Propagation measurement system and approach at 140 GHz- Moving to 6G and above 100 GHz," in *Proc. IEEE GLOBECOM*, Abu Dhabi, UAE, Dec. 2018, pp. 1–6.

[9] G. Lerosey, J. de Rosny, A. Tourin, A. Derode, G. Montaldo, and M. Fink, "Time reversal of electromagnetic waves," *Physical Review Lett.*, vol. 92, no. 19, p. 193904, 2004.

[10] R. C. Qiu, J. Q. Zhang, and N. Guo, "Detection of physics-based ultra-wideband signals using generalized RAKE with multiuser detection (MUD) and time-reversal mirror," *IEEE J. Sel. Areas Commun.*, vol. 24, no. 4, pp. 724–730, Apr. 2006.

[11] R. C. Qiu, C. Zhou, N. Guo, and J. Q. Zhang, "Time reversal with MISO for ultrawideband communications: Experimental results," *IEEE Ant. Wireless Prop. Lett.*, vol. 5, pp. 1–5, 2006.

[12] A. Mokh, R. Khayatzadeh, J. de Rosny, M. Kamoun, A. Ourir, A. Tourin, and M. Fink, "Indoor experimental evaluation of ultra-wideband MU-MISO TRDMA," in *Proc. IEEE VTC Spring*, Helsinki, Finland, Apr. 2021, pp. 1–5.

[13] A. Mokh, J. de Rosny, G. C. Alexandropoulos, R. Khayatzadeh, M. Kamoun, A. Ourir, A. Tourin, and M. Fink, "Time reversal for multiple access and mobility: Algorithmic design and experimental result," in *Proc. IEEE WCNC*, Austin, Texas, Apr. 2022, pp. 1–6.

[14] F. Han, Y.-H. Yang, B. Wang, Y. Wu, and K. J. Ray Liu, "Time-reversal division multiple access over multi-path channels," *IEEE Trans. Commun.*, vol. 60, no. 7, pp. 1953–1965, Jul. 2012.

[15] A. Mokh, J. de Rosny, G. C. Alexandropoulos, R. Khayatzadeh, A. Ourir, M. Kamoun, A. Tourin, and M. Fink, "Time reversal precoding at subTHz frequencies: Experimental results on spatiotemporal focusing," in *Proc. IEEE Conf. Standards Commun. Netw.*, Virtual, Dec. 2021, pp. 1–5.

[16] M. Fink, "Chaos and time-reversed acoustics," *Physics Today*, vol. 50, no. 3, pp. 34–40, Oct. 2001.

[17] G. C. Alexandropoulos, N. Shlezinger, and P. del Hougne, "Reconfigurable intelligent surfaces for rich scattering wireless communications: Recent experiments, challenges, and opportunities," *IEEE Commun. Mag.*, vol. 59, no. 6, pp. 28–34, Jun. 2021.